PCCP

PAPER

Cite this: *Phys. Chem. Chem. Phys.*, 2017, **19**, 8076

Ab initio study of aspirin adsorption on single-walled carbon and carbon nitride nanotubes

Yongju Lee,[a] Dae-Gyeon Kwon,†[a] Gunn Kim*[b] and Young-Kyun Kwon*[a]

Received 28th November 2016,
Accepted 16th February 2017

DOI: 10.1039/c6cp08122c

rsc.li/pccp

Using density functional theory, we investigate the adsorption properties of acetylsalicylic acid (aspirin) on the outer surfaces of a (10,0) carbon nanotube (CNT) and a (8,0) triazine-based graphitic carbon nitride nanotube (CNNT). The adsorption energies for the CNNT and CNT are 0.67 and 0.51 eV, respectively, and hence, the aspirin molecule binds more strongly to the CNNT. The stronger adsorption energy for the binding to the CNNT is ascribed to the high reactivity of its nitrogen atoms with high electron affinity. The CNNT exhibits local electric dipole moments that cause strong charge redistribution in the adsorbed aspirin molecule. The influence of an external electric field on the adsorption of aspirin on the nanotubes is explored by examining modifications in their electronic band structures, partial densities of states, and charge distributions. An electric field applied along a particular direction is found to induce molecular states of aspirin that lie within the in-gap region of the CNNT. This implies that the CNNT can be potentially utilized for the detection of aspirin.

1 Introduction

Acetylsalicylic acid (ASA), also known as aspirin, has been one of the most widely used medications in the world because of its well-known ability to reduce fevers and relieve aches and pains. Aspirin has been used to help prevent heart attack, stroke, and blood clot formation. Aspirin also suppresses prostaglandins owing to its ability to decrease platelet aggregation (antiplatelet effect), resulting in the inhibition of thrombus formation.[1] Moreover, aspirin has been reported to have anticancer properties[2] and is used as a precautionary medicine for stroke.[3] Despite its beneficial properties, the famous non-prescription medicine may be associated with some adverse effects. Consequently, there are warnings advising people to avoid its drug abuse and misuse. It is recommended that people with gastroenteric disorders, such as gastritis and peptic ulcers, seek medical advice before using aspirin, because aspirin may instigate stomach bleeding even in healthy individuals, especially when taken with alcohol. Therefore, it is important to be able to measure the amount of ASA in the human body.

There have been reported studies on aspirin adsorption on various surfaces. For instance, Abbasi *et al.* studied the adsorption energy of aspirin on a hydroxylated (001) α-quartz surface,[4] and Mphahlele *et al.* experimentally investigated the adsorption and removal of aspirin from aqueous solutions by using carbon nanotubes/β-cyclodextrin nanocomposites.[5] Few studies have, however, been performed on the detection of aspirin as well as its adsorption over various nanostructures such as carbon nanotubes.

Carbon nanotubes (CNTs) are thin, long tubular macromolecules formed from graphitic carbon. The discovery of CNTs[6] has attracted huge academic and industrial interest because of their unique physical and chemical properties,[7–17] to develop high performance devices. Researchers have been investigating the potential of CNTs in a wide range of applications: nanoelectronics, displays, batteries, polymer composites, and electrodes.[18–21] Recently, it has been reported that CNTs represent a new type of host sensor material capable of detecting small concentrations of various molecules with high sensitivity because of their unique characteristics. One of the attractive characteristics of a CNT is its very large adsorption surface area[22–24] compared to that of carbon-based adsorbents (such as activated carbon) used commercially. Its binding properties with several molecules have been studied theoretically and experimentally[25–31] to better understand their potential applications. Owing to their large adsorption surface area, CNTs can be used to filter or detect molecules. Since some molecules such as ammonia (NH_3),[32] nitrogen dioxide (NO_2),[32] alcohol,[33] and other molecules[34–37] have been reported to be detectable by CNT-based devices, a wide range of molecules have been studied for chemical sensing by CNTs. Owing to the

[a] *Department of Physics and Research Institute for Basic Sciences, Kyung Hee University, Seoul, 02447, Korea. E-mail: ykkwon@khu.ac.kr*
[b] *Department of Physics & Astronomy and Graphene Research Institute, Sejong University, Seoul, 05006, Korea. E-mail: gunnkim@sejong.ac.kr*
† Current address: LG Chem Research Park, Daejeon 34122, Korea.

modification of the intrinsic electronic structures of semiconducting CNTs by adsorption, it is possible to detect the type and concentration of specific target molecules.

Carbon nitride compounds have been studied in various areas such as in electronic devices, humidity sensors, and coatings because of their electronic and chemical properties.[38–40] Their structures vary depending on the carbon to nitrogen atomic ratio and arrangement. In this study, we focus on a triazine-based graphitic carbon nitride (g-C_3N_4) nanotube (CNNT). Recent studies have reported the synthesis of the g-C_3N_4 nanotube, as well as *ab initio* calculations.[41–44] Various adsorption properties are expected because of the unique porous structure of the CNNT.

In this paper, we present a first-principles study of the binding properties of ASA on a bare CNT and a bare CNNT. We found that ASA binds to pristine CNT (CNNT) with a binding energy of 0.51 eV (0.67 eV), and no practical charge transfer takes place. According to our analyses of the electronic structure, the ASA-adsorbed CNT does not show significantly different characteristics from the bare CNT; on the other hand, the analogous ASA-adsorbed CNNT is noticeably different from those of the bare CNNT. Because of the structure of the CNNT, local electric dipole moments are created, which interrupt the exchange of electrons between the ASA molecule and the CNNT. Finally we discuss the effects of a homogeneous external electric field (E-field) on the ASA-adsorbed CNNT. The response of the nanotube to the E-field is appealing for its application to electric devices.

2 Computational details

Using a computational study based on density functional theory (DFT),[45,46] we examined the CNT and the CNNT with respect to the adsorption of ASA. Electronic wavefunctions were expanded into plane waves to a cutoff energy of 450 eV, and the ion–electron interactions were described using the projector augmented wave method implemented in the Vienna *ab initio* simulation package (VASP),[47,48] within the generalized gradient approximation (GGA) method.[49] To better describe the interaction between ASA and nanotubes, we included van der Waals interaction using Grimme's method (DFT-D2).[50] All the model structures were optimized until the Hellmann–Feynman forces were less than 0.03 eV Å^{-1}.

We chose host materials for molecular adsorption that satisfy the following two conditions. One is that sensor applications require semiconductor devices, and we focused only on semiconducting nanotubes. The other is that nanotubes should not only be large enough to be observed or synthesized experimentally, but should also be small enough for computational calculations. Hence, we chose a (10,0) CNT and a (8,0) CNNT as host materials for molecular adsorption.

For the calculation of the ASA molecule in a vacuum, we used a cubic supercell with a length of 30 Å. The Γ point was used in the calculations of the isolated ASA molecule. For the systems containing nanotubes, we also used supercells with lengths of 16.05 Å for the CNT, and 15.72 Å for the CNNT, respectively, along the tube axis and 30 Å along the other two lateral directions. After a careful convergence test of the k-point sampling, we used the Γ point and 10 k points in the axial direction for the geometry optimization and the electronic structure calculations, respectively.

For each adsorption configuration, we calculated the binding energy (E_b) defined as

$$E_b = E[\text{tube} + \text{ASA}] - (E[\text{tube}] + E[\text{ASA}]), \quad (1)$$

where E[tube + ASA] is the total energy of the CNT or the CNNT bound to an ASA molecule, E[tube] is the total energy of each nanotube without an ASA molecule, and E[ASA] is the energy of the isolated ASA molecule, respectively.

To explore the E-field effect, we generated the E-field by applying a sawtooth-shaped potential along a certain periodic direction. In order to prevent the effect of discontinuity of the sawtooth potential, we can only apply an E-field along non-periodic directions containing a vacuum region between neighboring supercells. We also performed the geometry optimization under an external electric field.

3 Results and discussion

Fig. 1(a) shows the most stable structure of the ASA molecule ($C_9H_8O_4$) in a vacuum. It consists of an aromatic ring, ester, and carboxylic acid. Fig. 1(b) shows its highest occupied molecular orbital (HOMO) and lowest unoccupied molecular orbital (HOMO). Its HOMO–LUMO gap is calculated to be 3.75 eV. In both the HOMO and the LUMO of ASA, the electron densities are distributed over the entire molecule, as shown in Fig. 1(b). Two types of nanotubes were chosen for the investigation of their ability to detect ASA molecules: the (10,0) CNT and the (8,0) CNNT. As shown in Fig. 2(a) and (b), the bare (10,0) CNT was calculated to have a band gap of 0.88 eV, while the band gap of the bare (8,0) CNNT was calculated to be 2.73 eV. These calculated band gaps are in good agreement with previous results.[51,52] The ASA-adsorbed (10,0) CNT and the ASA-adsorbed (8,0) CNNT were also calculated to have band gaps of 0.87 and 2.66 eV, respectively.

When an ASA molecule is adsorbed on a nanotube, many configurations are possible. After exploring various configurations, we found that π–π stacking configurations are more stable

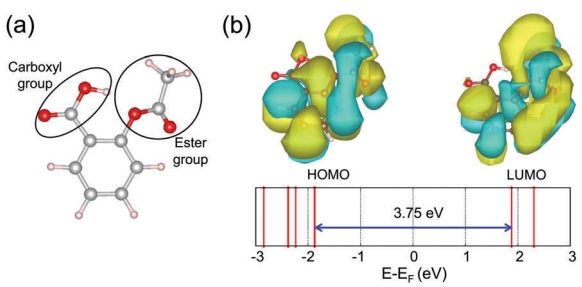

Fig. 1 (a) Model structure of an ASA molecule. (b) Electronic energy levels of an ASA molecule showing the HOMO and LUMO wavefunctions. The HOMO–LUMO gap is 3.75 eV.

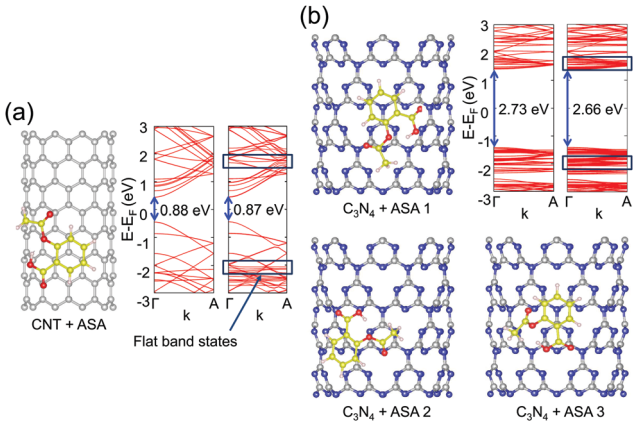

Fig. 2 Atomic structures and electronic bands of ASA-adsorbed (a) CNT and (b) CNNT. The lowest energy adsorption sites among the possible configurations (left) and the band structures of the bare nanotube (middle) and the ASA-bound nanotube (right). The flat bands in the rectangles originate from the ASA molecule adsorbed on the tube.

compared to the other stacking configurations. In this study, therefore, we show and discuss only π–π stacking configurations. The total energy of each configuration was computed to obtain the lowest energy adsorption site. For visual clarity, the carbon atoms of the ASA molecule in Fig. 2 are shown in yellow, while those of the CNT and the CNNT are represented in black. When ASA is bound to the (10,0) CNT, the lowest energy configuration resembles that of Bernal stacking (AB stacking) in graphite, as can be seen in Fig. 2(a). The electronic band structure of the ASA-adsorbed CNT shows no clear change near the Fermi level compared with that of the bare CNT, even when flat bands, of around −2 and +2 eV, originating from the ASA molecule, are considered. Fig. 2(b) shows the three lowest energy binding structures of the CNNT with an ASA adsorbate. The band gap of the CNNT decreases by about 70 meV when ASA is bound to the CNNT. Since π–π interaction is mainly responsible for the molecular binding, a noticeable charge transfer does not occur. Consequently, no molecular state of ASA contributes to the band gap of either the CNT or the CNNT. We conclude that it would be difficult to detect ASA using a CNT or a CNNT in the absence of an external E-field. Table 1 summarizes the adsorption energy and the distance between the ASA molecule and the tube wall for each adsorption configuration. We find that ASA binds more strongly to the CNNT over the CNT. To check the dependence of the binding energy on the tube diameter, we also performed first-principles calculations of aspirin adsorption on a (16,0) CNT and a (5,0) CNNT, which have similar diameters to a (8,0) CNNT and a (10,0) CNT, respectively. Our calculation shows that indeed

Table 1 The binding energy and distance between the adsorbed molecule and nanotubes

Structure	Binding energy (eV)	Distance (Å)
CNT + ASA	−0.54	2.59
C_3N_4 + ASA 1	−0.66	2.70
C_3N_4 + ASA 2	−0.68	2.68
C_3N_4 + ASA 3	−0.67	2.72

Table 2 Comparison of the binding energies (B.E.) of an ASA molecule on CNTs and CNNTs with similar diameters (*D*)

D (Å)	Structure	B.E. (eV)	Structure	B.E. (eV)
7.8	C_3N_4 (5,0) + ASA	−0.61	CNT (10,0) + ASA	−0.54
12.2	C_3N_4 (8,0) + ASA	−0.67	CNT (16,0) + ASA	−0.58

ASA adsorption on the CNNT is stronger than that on the CNT, as summarized in Table 2.

To understand this difference in adsorption energy, we examined the interaction between the ASA molecule and the CNT and CNNT in further detail. Fig. 3(a) and (b) show charge difference plots [ρ(tube + ASA) − ρ(tube) − ρ(ASA)] for two ASA-adsorbed nanotubes: the (10,0) CNT and the (8,0) CNNT, respectively. ρ(tube + ASA) indicates the charge density of ASA adsorbed nanotubes. ρ(ASA) and ρ(tube) indicate the charge densities of only ASA and nanotubes, respectively. These differences show charge difference caused by adsorption. As shown in Fig. 3(a), the electrons in the ASA molecule tend to move away from the CNT as the cyan and yellow colors seem to split, whereas from Fig. 3(b), the cyan and yellow colors seem to be much more mixed, implying a more complicated charge redistribution in the ASA molecule on the CNNT. As mentioned above, there is no charge transfer between the ASA molecule and either nanotube. Interestingly, we observe that a much greater charge redistribution is observed in the ASA molecule bound to the CNNT than in the ASA molecule bound to the CNT. What is

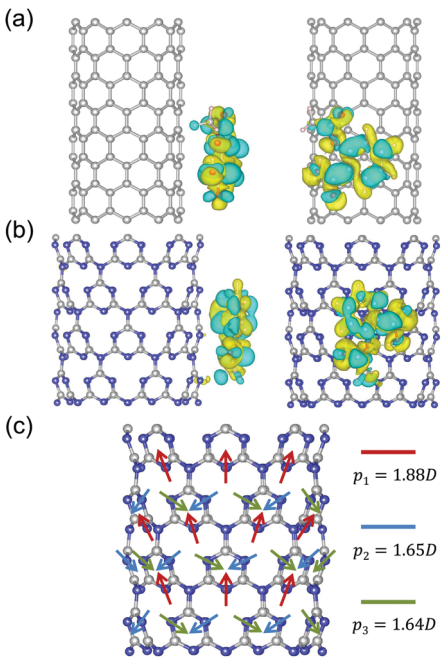

Fig. 3 Two different views of charge density differences between (a) the bare CNT and the ASA-adsorbed CNT, and (b) the bare CNNT and the ASA-adsorbed CNNT. Cyan and yellow colors represent electron accumulation and electron depletion, respectively. (c) Local electric dipole moments in the pristine CNNT are given in Debye (D): red, blue and green arrows indicate different types of local electric dipole moments. Carbon and nitrogen atoms are denoted by gray and blue balls.

responsible for charge redistribution in ASA? Because of the electronic configuration of the C and N atoms, the CNNT forms a buckled structure in contrast to the CNT. Lone-pair electrons, which are localized at the N atoms, result in buckling of the tube surface. In addition, local electric dipole moments within the CNNT are also involved in charge redistribution in the ASA molecule. The differences in the electron affinities of the C and N atoms cause the local electric dipole moments, which are expressed by eqn (2). Electric dipole moments within the CNNT are shown in Fig. 3(c). These local electric dipole moments, together with buckling and vacancies, bring about the charge redistribution observed when ASA is bound to the CNNT.

$$\mathbf{p}(\mathbf{r}) = \int_V \rho(\mathbf{r}')(\mathbf{r}' - \mathbf{r})\mathrm{d}\mathbf{r}', \qquad (2)$$

where $\mathbf{r}$ locates the point of observation, d$\mathbf{r}$ indicates an infinitesimal volume in V, and ρ is the charge density. V is selected as a local volume which has the same amount of electron charge as a neutral isolated N atom in the CNNT. There is charge accumulation around the N atom caused by the electronegativity difference between C and N atoms in the CNNT. $\rho(\mathbf{r})$ is the charge density within this local volume.

Fig. 3(c) depicts the local electric dipole moments on the surface of the CNNT. It should be noted that the nitrogen atoms with red arrows are more severely buckled in different directions from those with green and blue arrows. The dipole moments denoted by green and blue arrows have almost identical values of 1.64 D and 1.65 D (1 D $\approx$ 3.336 $\times$ 10^{-30} C m $\approx$ 0.2082 e Å), respectively, while those with red arrows are larger (1.88 D). As a result of the local electric dipole moments, the ASA molecule interacts with the CNNT through dipole–dipole interaction. ASA in a vacuum has an electric dipole moment of 1.51 D, but ASA bound to the CNNT has a larger electric dipole moment of 2.25 D. If a simple dipole–dipole interaction (V_{dd} in eqn (3)) is applied with the aforementioned dipole moments, the interaction energy is calculated to be about -0.1 eV; this explains the difference in the binding energies listed in Table 1. We conclude that the aspirin molecule binds more strongly on the CNNT than the CNT owing to the dipole–dipole interaction

$$V_{\mathrm{dd}} = \frac{1}{4\pi\varepsilon_0}\left[\frac{\vec{p}_1 \cdot \vec{p}_2}{|\vec{r}_1 - \vec{r}_2|^3} - \frac{3\{(\vec{r}_1 - \vec{r}_2)\cdot\vec{p}_1\}\{(\vec{r}_1 - \vec{r}_2)\cdot\vec{p}_2\}}{|\vec{r}_1 - \vec{r}_2|^5}\right], \qquad (3)$$

where V_{dd} is a potential energy for dipole–dipole interaction, and $\vec{p}_i$ and $\vec{r}_i$ (i = 1, 2) are the i-th electric dipole moment and its position, respectively.

To check whether the nanotubes can be applied in devices for detecting ASA molecules, we investigated the effects of external E-fields on the electronic properties of the bare CNNT as well as the ASA-adsorbed CNNT. In a single-gated field effect transistor, the E-field is generated by an applied bias between a gate and a nanotube. Our computational results reveal differences between the electronic structure of the bare CNNT and the ASA-adsorbed CNNT. In particular, the band gap of the bare CNNT is calculated to be much smaller than that of the ASA-adsorbed CNNT.

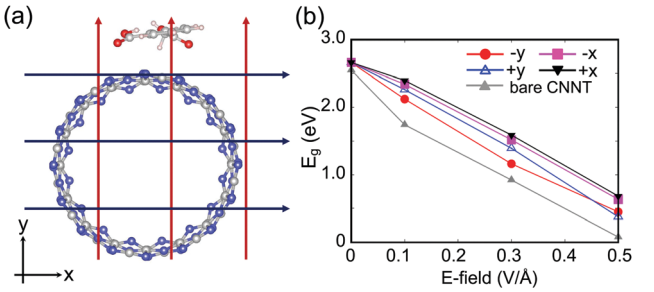

Fig. 4 (a) External electric field on the ASA-adsorbed CNNT. (b) Band gaps for the bare CNNT and the ASA-adsorbed CNNT as a function of the external electric field direction. The x direction is also perpendicular to the CNNT, but horizontal to the ASA molecule. The y direction is perpendicular to both the ASA molecule and the CNNT.

Not only is there a difference in the band gap but there are also different electronic properties in four directions. The electronic structure of the ASA-adsorbed CNNT is not affected much by an E-field perpendicular to the tube axis. In contrast, the ASA-adsorbed CNNT shows remarkable characteristics in its band structure that are dependent on the direction of the transverse E-field, as shown in Fig. 4. We chose four directions for the E-field ($\pm x$ and $\pm y$), which were all perpendicular to the CNNT axis. E-fields in $\pm y$ directions enhance the electronic coupling between the ASA molecule and the CNNT, whereas

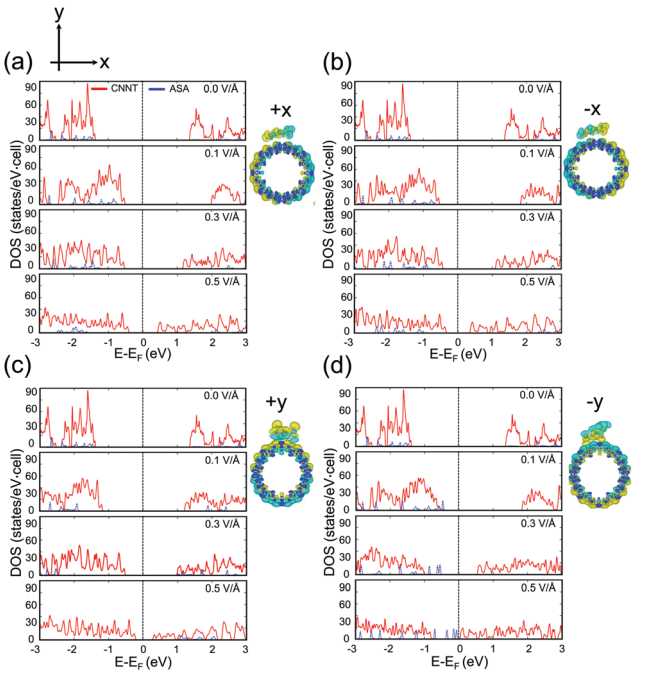

Fig. 5 (a–d) PDOS plots and electron density differences of the ASA-adsorbed CNNT under the external E-fields in $+x$, $-x$, $+y$ and $-y$ directions, respectively. The arrows indicate the directions of the E-fields. Red lines indicate the PDOS of the CNNT and blue lines indicate the PDOS of the ASA molecule, respectively. Charge transfer only occurs when the external E-field is applied. Cyan and yellow colors represent electron accumulation and electron depletion, respectively.

fields applied in the $\pm x$ directions show only weak ASA–CNNT coupling. Fig. 4(b) shows that the external E-field can modulate the electronic structure of the ASA-adsorbed CNNT.

The partial densities of states (PDOS) of the ASA-adsorbed CNNT were determined, and are shown in Fig. 5. As the CNNT has a higher electric potential than the ASA adsorbate, when an E-field is applied in the $-y$ direction, electrons are donated from the adsorbed ASA molecule to one part of the CNNT. Fig. 5(a) shows that as the strength of the transverse E-field in the $-y$ direction increases, the localized states of the ASA molecule are upshifted. At the same time, the conduction band of the tube moves down toward the Fermi level. On the other hand, E-fields applied in $+y$ and $\pm x$ directions have similar effects; the band gap decreases, but the states originating from ASA do not appear as in-gap states. In both $\pm x$ directions, the external E-field does not cause a strong ASA–CNNT coupling enhancement, which is a consequence of reflection symmetry. It is well-known that DFT may give incorrect gap values, especially for insulators and molecules, but the tendency of the HOMO state moving toward the in-gap region under the E-field in the $-y$ direction may still be valid. The band gap of the bare CNNT is also reduced under an external E-field, but there is no localized state in the energy band gap in this case. Under the real conditions, the CNNT would be randomly coated with ASA molecules, and hence, any E-field direction results in ASA states that occur within the forbidden band. Such in-gap states could give rise to the scattering in the electron transport, which would be experimentally reflected in the current–voltage curve. Consequently, a C_3N_4 nanotube-based sensor device could detect ASA molecules using a gate bias voltage (or an external E-field).

4 Conclusions

We performed *ab initio* calculations to investigate the adsorption properties of an aspirin molecule on a CNT and a CNNT. Considering various adsorption configurations, it was found that aspirin is more strongly bound to the CNNT than to the CNT with a similar diameter. For instance, $E_b = -0.68$ eV for a (8,0) CNNT and $E_b = -0.58$ eV for a (16,0) CNT. We assigned such binding enhancement on CNNTs to the intrinsic local electric dipole moments existing in CNNTs due to the electronegativity difference and structural properties of the C and N atoms, resulting in the dipole–dipole interaction between the CNNT and the ASA molecule. When a homogeneous external electric field is introduced, the band gap in the CNNT decreases dramatically in the presence of the aspirin adsorbates, especially when the E-field is applied in the $-y$ direction, resulting in the in-gap states of the aspirin molecule. This result indicates that CNNTs may be used to detect ASA molecules in the presence of an external E-field showing that CNNT-based field effect transistors could be equipped with aspirin sensors. To obtain more concrete results, we plan to investigate the electronic properties of ASA adsorption on the CNT and CNNT in a solution environment, as well as the charge transport.

Acknowledgements

We gratefully acknowledge financial support from the National Research Foundation (NRF-2015R1A2A2A01006204), the Future Semiconductor Device Technology Development Program (Project No. 10045360), and the KSRC (Korea Semiconductor Research Consortium). GK were supported by the Priority Research Center Program (Grant No. 2010-0020207) and the Mid-career Researcher Program (Grant No. 2016R1A2B2016120) through the NRF grant funded by the MEST. Some portion of our computational work was done using the resources of the KISTI Supercomputing Center (KSC-2016-C3-0034).

References

1 T. O. Cheng, *Texas Heart Inst. J.*, 2007, **34**, 392–393.
2 S. H. Ferreira, S. Moncada and J. R. Vane, *Br. J. Pharmacol.*, 1973, **49**, 86–97.
3 H. D. Lewis, J. W. Davis, D. G. Archibald, W. E. Steinke, T. C. Smitherman, J. E. Doherty, H. W. Schnaper, M. M. LeWinter, E. Linares, J. M. Pouget, S. C. Sabharwal, E. Chesler and H. DeMots, *N. Engl. J. Med.*, 1983, **309**, 396–403.
4 A. Abbasi, E. Nadimi, P. Plänitz and C. Radehaus, *Surf. Sci.*, 2009, **603**, 2502–2506.
5 K. Mphahlele, M. S. Onyango and S. D. Mhlanga, *J. Environ. Chem. Eng.*, 2015, **3**, 2619–2630.
6 S. Iijima, *Nature*, 1991, **354**, 56–58.
7 L. Chico, V. Crespi, L. Benedict, S. Louie and M. Cohen, *Phys. Rev. Lett.*, 1996, **76**, 971–974.
8 S. J. S. Tans, A. R. M. A. Verschueren and C. Dekker, *Nature*, 1998, **393**, 49–52.
9 Y.-K. Kwon, D. Tomanek and S. Iijima, *Phys. Rev. Lett.*, 1999, **82**, 1470–1473.
10 Z. Yao, H. W. Ch. Postma, L. Balents and C. Dekker, *Nature*, 1999, **402**, 273–276.
11 S. Sanvito, Y.-K. Kwon, D. Tománek and C. J. Lambert, *Phys. Rev. Lett.*, 1999, **84**, 1974–1977.
12 S. Berber, Y.-K. Kwon and D. Tomanek, *Phys. Rev. Lett.*, 2000, **84**, 4613–4616.
13 C. Zhou, J. Kong, E. Yenilmez and H. Dai, *Science*, 2000, **290**, 1552–1555.
14 J. Lee, H. Kim, S.-J. Kahng, G. Kim, Y.-W. Son, J. Ihm, H. Kato, Z. W. Wang, T. Okazaki, H. Shinohara and Y. Kuk, *Nature*, 2002, **415**, 1005–1008.
15 G. Kim, S. B. Lee, T.-S. Kim and J. Ihm, *Phys. Rev. B: Condens. Matter Mater. Phys.*, 2005, **71**, 205415.
16 J.-C. Charlier, X. Blase and S. Roche, *Rev. Mod. Phys.*, 2007, **79**, 677–732.
17 W. I. Choi, J. Ihm and G. Kim, *Appl. Phys. Lett.*, 2008, **92**, 1–3.
18 H. Dai, *Surf. Sci.*, 2002, **500**, 218–241.
19 P. M. Ajayan and O. Z. Zhou, *Top. Appl. Phys.*, 2001, **425**, 391–425.
20 M. S. Dresselhaus and H. Dai, *MRS Bull.*, 2004, **29**, 237–243.
21 R. H. Baughman, A. A. Zakhidov and W. A. de Heer, *Science*, 2002, **297**, 787–793.

22 R. Q. Long and R. T. Yang, *Ind. Eng. Chem. Res.*, 2001, **40**, 4288–4291.
23 M. Cinke, J. Li, B. Chen, A. Cassell, L. Delzeit, J. Han and M. Meyyappan, *Chem. Phys. Lett.*, 2002, **365**, 69–74.
24 Y. F. Yin, T. Mays and B. McEnaney, *Langmuir*, 2000, **16**, 10521–10527.
25 A. C. Dillon, K. M. Jones, T. A. Bekkedahl, C. H. Kiang, D. S. Bethune and M. J. Heben, *Nature*, 1997, **386**, 377–379.
26 A. Chambers, C. Park, R. T. K. Baker and N. M. Rodriguez, *J. Phys. Chem. B*, 1998, **102**, 4253–4256.
27 R. Q. Long and R. T. Yang, *J. Am. Chem. Soc.*, 2001, **123**, 2058–2059.
28 X. Peng, Y. Li, Z. Luan, Z. Di, H. Wang, B. Tian and Z. Jia, *Chem. Phys. Lett.*, 2003, **376**, 154–158.
29 S. B. Fagan, A. G. Souza Filho, J. O. G. Lima, J. Mendes Filho, O. P. Ferreira, I. O. Mazali, O. L. Alves and M. S. Dresselhaus, *Nano Lett.*, 2004, **4**, 1285–1288.
30 S. B. Fagan, E. C. Girão, J. M. Filho and A. G. S. Filho, *Int. J. Quantum Chem.*, 2006, **106**, 2558–2563.
31 F. Tournus, S. Latil, M. Heggie and J.-C. Charlier, *Phys. Rev. B: Condens. Matter Mater. Phys.*, 2005, **72**, 075431.
32 J. Kong, *Science*, 2000, **287**, 622–625.
33 H. J. Song, Y. Lee, T. Jiang, A. G. Kussow, M. Lee, S. Hong, Y.-K. Kwon and H. C. Choi, *J. Phys. Chem. C*, 2008, **112**, 629–634.
34 P. G. Collins, *Science*, 2000, **287**, 1801–1804.
35 K. Bradley, J. C. P. Gabriel, A. Star and G. Grüner, *Appl. Phys. Lett.*, 2003, **83**, 3821–3823.
36 M.-F. Yu, B. S. Files, S. Arepalli and R. S. Ruoff, *Phys. Rev. Lett.*, 2000, **84**, 5552–5555.
37 D. P. Burt, N. R. Wilson, J. M. R. Weaver, P. S. Dobson and J. V. Macpherson, *Nano Lett.*, 2005, **5**, 639–643.
38 Y. Zhang, A. Thomas, M. Antonietti and X. Wang, *J. Am. Chem. Soc.*, 2009, **131**, 50–51.
39 D. Li, X. Chu, S.-C. Cheng, X.-W. Lin, V. P. Dravid, Y.-W. Chung, M.-S. Wong and W. D. Sproul, *Appl. Phys. Lett.*, 1995, **67**, 203.
40 B. L. M. Zambov, C. Popov, N. Abedinov, M. F. Plass, W. Kulisch, T. Gotszalk, P. Grabiec, I. W. Rangelow and R. Kassing, *Adv. Mater.*, 2000, **12**, 656–660.
41 C. Cao, F. Huang, C. Cao, J. Li and H. Zhu, *Chem. Mater.*, 2004, **16**, 5213–5215.
42 Q. Guo, Y. Xie, X. Wang, S. Zhang, T. Hou and S. Lv, *Chem. Commun.*, 2004, 26–27.
43 J. Li, C. Cao and H. Zhu, *Nanotechnology*, 2007, **18**, 115605.
44 H. Pan, Y.-W. Zhang, V. B. Shenoy and H. Gao, *Nanoscale Res. Lett.*, 2011, **6**, 97.
45 P. Hohenberg and W. Kohn, *Phys. Rev. B: Solid State*, 1964, **136**, B864–B871.
46 W. Kohn and L. J. Sham, *Phys. Rev.*, 1965, **140**, A1133–A1138.
47 G. Kresse and J. Hafner, *Phys. Rev. B: Condens. Matter Mater. Phys.*, 1993, **47**, 558–561.
48 G. Kresse, *Phys. Rev. B: Condens. Matter Mater. Phys.*, 1996, **54**, 11169–11186.
49 J. Perdew, K. Burke and M. Ernzerhof, *Phys. Rev. Lett.*, 1996, **77**, 3865–3868.
50 S. Grimme, *J. Comput. Chem.*, 2006, **27**, 1787–1799.
51 F. Shojaei and H. S. Kang, *RSC Adv.*, 2015, **5**, 10892–10898.
52 B. Kozinsky and N. Marzari, *Phys. Rev. Lett.*, 2006, **96**, 2–5.